AIAA JOURNAL
Vol. 49, No. 4, April 2011

Technical Notes

Improved Aerodynamic Model for Efficient Analysis of Flapping-Wing Flight

Dae-Kwan Kim*
Korea Aerospace Research Institute, Daejeon 305-333, Republic of Korea
and
Jun-Seong Lee† and Jae-Hung Han‡
Korea Advanced Institute of Science and Technology, Daejeon 305-701, Republic of Korea

DOI: 10.2514/1.J050556

Nomenclature

c	=	wing section chord
$(C_d)_{\text{cf}}$	=	drag coefficient due to crossflow
$(C_d)_f$	=	drag coefficient due to friction
D_{camber}	=	chordwise force due to camber
D_f	=	chordwise friction drag
$\mathrm{d}y$	=	spanwise length of a particular wing section
$\dot{h}$	=	plunging or heaving velocity of wing section
N_a	=	normal force due to apparent mass effect
N_c	=	circulatory normal force
T_s	=	leading-edge suction force
U	=	freestream velocity or inflow velocity
$\hat{V}_{0.25c}$	=	resultant velocity at quarter-chord location
w	=	downwash velocity
$\bar{\alpha}$	=	resultant angle of attack, $\theta + \tan^{-1}(\dot{h}/U)$
α_0	=	section zero-lift angle of attack
$\delta\theta$	=	zero mean dynamic pitch angle
η_s	=	leading-edge suction efficiency
θ	=	pitch angle, $\bar{\theta} + \delta\theta$
$\dot{\theta}$	=	pitching velocity of wing section
$\bar{\theta}$	=	total mean pitch angle
$\bar{\theta}_a$	=	mean pitch angle of flapping axis with respect to U
ρ	=	atmospheric density

I. Introduction

THE fluid–structure interaction analysis of biological and artificial flapping flyers is extremely complicated; thus, an efficient unsteady aerodynamic model is required in such time-consuming problems as optimal flapping-wing design and flapping-wing flight simulation. In spite of the remarkable achievements in flapping-wing aerodynamic modeling, most studies on the flight dynamics and control of ornithopters have been performed by employing quasi-steady models [1–5]. These aerodynamic models cannot describe the unique aerodynamic characteristics of ornithopter flights in low Reynolds numbers, such as wake effect and dynamics stall. DeLaurier [6] developed an efficient unsteady aerodynamic model of a root flapping wing by using a modified strip theory (MST) in terms of a three-dimensional Theodorsen function with the consideration of leading-edge suction force, poststall phenomena, friction drag, and vortex wake effect.

The purpose of this Note is to further improve MST to consider dynamic stall for a high relative angle of attack. The analysis results of the present aerodynamic model are compared with the experimental data of a flat plate wing with oscillating motion.

Received 15 March 2010; revision received 6 October 2010; accepted for publication 15 December 2010.

*Senior Researcher, Satellite Control System Department; dkk@kari.re.kr.
†Graduate Research Assistant, Department of Aerospace Engineering; jsl1009@kaist.ac.kr. Student Member AIAA.
‡Associate Professor, Department of Aerospace Engineering; jaehunghan@kaist.ac.kr. Senior Member AIAA.

II. Aerodynamic Model

A. High Relative Angle of Attack

MST was originally derived under the approximations that the wing section has a small relative angle of attack. However, if the plunging velocity is increased relative to the freestream velocity, then the wing section could be exposed to a high relative angle of attack. This means that MST no longer stands for the low-order approximations to express the nonlinear terms inside the aerodynamic model. Therefore, we took the higher-order approximation into account to expand the aerodynamic model for a high relative angle of attack.

With the horizontal velocity V_x and the vertical velocity $V_{n,0.25c}$ of the wing section at the quarter-chord location, as shown in Fig. 1, the relative angle of attack can be defined as follows:

$$\gamma = \tan^{-1}(V_{n,0.25c}/V_x) = \tan^{-1}\left[\frac{\dot{h}\cos(\theta-\bar{\theta}_a) + 0.25c\dot{\theta} + U\sin\theta - w}{U\cos\theta - \dot{h}\sin(\theta-\bar{\theta}_a)}\right] \quad (1)$$

In Eq. (1), $\sin\theta$ can be expressed by using a trigonometric series as follows:

$$\sin\theta = \delta\theta + \bar{\theta} + \mathcal{O}(\theta^3) \quad (2)$$

where the last term represents the sum of higher-order terms.

With the flow's relative angle of attack at the $\frac{3}{4}$-chord location α', given in [6], and Eq. (2), the vertical velocity component at the quarter-chord location can be expressed as follows:

$$V_{n,0.25c} = U\left[\frac{\dot{h}\cos(\theta-\bar{\theta}_a) + 0.75c\dot{\theta} + U\delta\theta - w}{U}\right] + U[\bar{\theta} + \mathcal{O}(\theta^3)] - 0.5c\dot{\theta} = U[\alpha' + \bar{\theta} + \mathcal{O}(\theta^3)] - 0.5c\dot{\theta} \quad (3)$$

The relative angle of attack γ can be obtained by

$$\gamma = \tan^{-1}\left[\frac{U\alpha' + U(\bar{\theta} + \mathcal{O}(\theta^3)) - 0.5c\dot{\theta}}{U\cos\theta - \dot{h}\sin(\theta-\bar{\theta}_a)}\right] \quad (4)$$

Taking into account the relative angle of attack in Eq. (4), the section's circulatory normal force, the leading-edge suction force, and the chordwise force due to the camber can be expressed as

$$\mathrm{d}N_c = 2\pi(\alpha' + \alpha_0 + \bar{\theta})\cos\gamma\frac{\rho U\hat{V}_{0.25c}}{2}c\mathrm{d}y \tag{5}$$

$$\mathrm{d}T_s = \eta_s 2\pi\left(\alpha' + \bar{\theta} - \frac{1}{4}\frac{c\dot{\theta}}{U}\right)\sin\gamma\frac{\rho U\hat{V}_{0.25c}}{2}c\mathrm{d}y \tag{6}$$

$$\mathrm{d}D_{\mathrm{camber}} = -2\pi\alpha_0(\alpha' + \bar{\theta})\cos\gamma\frac{\rho U\hat{V}_{0.25c}}{2}c\mathrm{d}y \tag{7}$$

Eq. (9), $(\alpha_{\mathrm{dynamic}})_{\min}$ and $(\alpha_{\mathrm{dynamic}})_{\max}$ are the minimum and maximum dynamic stall angles, which are available over the attached flow condition and are expressed as follows:

$$(\alpha_{\mathrm{dynamic}})_{\max} = \xi_{\max}(\alpha_{\mathrm{stall}})_{\max} \tag{10a}$$

$$(\alpha_{\mathrm{dynamic}})_{\min} = \xi_{\min}(\alpha_{\mathrm{stall}})_{\min} \tag{10b}$$

with

$$\xi_{\max} = \begin{cases} 1 + \frac{|\tan^{-1}[\dot{h}\cos(\theta-\bar{\theta}_a)/V_x]|}{|(\alpha_{\mathrm{stall}})_{\max}|} + \frac{0.51(\theta/\dot{\theta}_{\mathrm{mag}})\sqrt{c\dot{\theta}_{\mathrm{mag}}/2U}}{(\alpha_{\mathrm{stall}})_{\max}}, & (\alpha_{\mathrm{dynamic}})_{\max} \le 2(\alpha_{\mathrm{stall}})_{\max} \\ 2, & (\alpha_{\mathrm{dynamic}})_{\max} > 2(\alpha_{\mathrm{stall}})_{\max} \end{cases} \tag{11a}$$

$$\xi_{\min} = \begin{cases} 1 + \frac{|\tan^{-1}[\dot{h}\cos(\theta-\bar{\theta}_a)/V_x]|}{|(\alpha_{\mathrm{stall}})_{\min}|} + \frac{0.51(\theta/\dot{\theta}_{\mathrm{mag}})\sqrt{c\dot{\theta}_{\mathrm{mag}}/2U}}{(\alpha_{\mathrm{stall}})_{\min}}, & (\alpha_{\mathrm{dynamic}})_{\min} \ge 2(\alpha_{\mathrm{stall}})_{\min} \\ 2, & (\alpha_{\mathrm{dynamic}})_{\min} < 2(\alpha_{\mathrm{stall}})_{\min} \end{cases} \tag{11b}$$

where $\dot{\theta}_{\mathrm{mag}}$ is the absolute value of $\dot{\theta}$ [10]. As expressed by Eq. (11), the dynamic stall criteria depend on both the plunging and pitching effects.

The other aerodynamic forces, $\mathrm{d}N_a$ and $\mathrm{d}D_f$, are the same as given by Eqs. 14 and 19 in [6], respectively.

B. Dynamic Stall Model

Unsteady dynamic stall effects were observed in the high relative angle of attack ranges caused by the large plunging motion as well as by the pitching motion [7]; thus, the dynamic stall effect due to the plunging motion, and not just for the pitching motion, needs to be considered in the aerodynamic model. In the MST model, as expressed by Eq. 22 in [6], the effects of pitching and plunging are reflected in a dynamic stall model through the rate of change of the angle of attack. However, the stall model is not adequate to flapping-wing flight with large plunging and pitching motions in low Reynolds number flow, because the dynamic stall angle was taken from the semiempirical criteria for helicopters [8].

The dynamic stall model proposed in this study consists of two parts: 1) when the dynamic stall effect occurs (the dynamic stall criteria), and 2) how the magnitude of aerodynamic forces is determined (the dynamic stall effect). The dynamic stall criteria can be formulated based on the unsteady aerodynamic test data of the flapping wing. However, it is not easy to define the representative stall criteria in closed form. In the present study, based on the experimental data acquired by Scherer [9], we adopt the dynamic stall effect, as in the following statement: the instantaneous maximum values of the lift coefficient could be as large as twice the maximum steady value under the dynamic stall criteria. Using the assumption of dynamic stall phenomena and the relative angle of attack γ expressed in Eq. (4), we suggest here the dynamic stall criteria defined at the leading edge of the flapping wing as follows:

1) For the attached flow condition,

$$(\alpha_{\mathrm{stall}})_{\min} \le \left[\gamma - \frac{1}{4}\left(\frac{c\dot{\theta}}{U}\right)\right] \le (\alpha_{\mathrm{stall}})_{\max} \tag{8}$$

2) For the dynamic stall condition,

$$(\alpha_{\mathrm{dynamic}})_{\min} \le \left[\gamma - \frac{1}{4}\left(\frac{c\dot{\theta}}{U}\right)\right] \le (\alpha_{\mathrm{dynamic}})_{\max} \tag{9}$$

3) Poststall condition is defined beyond the dynamic stall range. In Eq. (8), $(\alpha_{\mathrm{stall}})_{\min}$ and $(\alpha_{\mathrm{stall}})_{\max}$ are the minimum and maximum static stall angles determined in the steady aerodynamic data. In

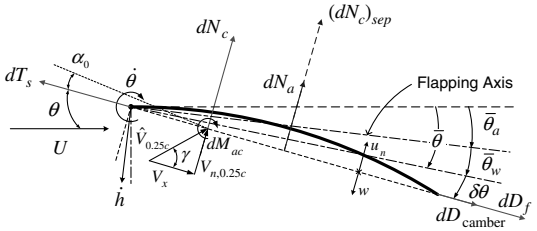

Fig. 1 Wing section aerodynamic forces and motion variables.

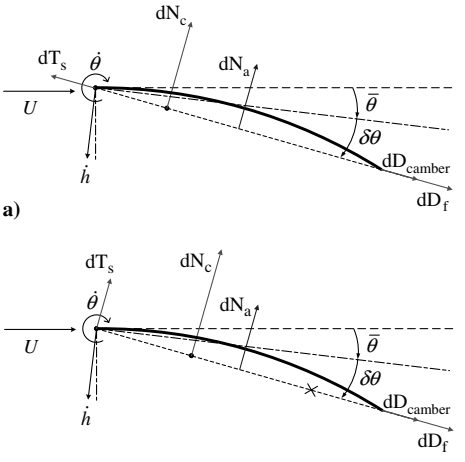

Fig. 2 Wing section aerodynamic forces according to the stall conditions: a) attached flow range, b) dynamic stall range, and c) poststall range.

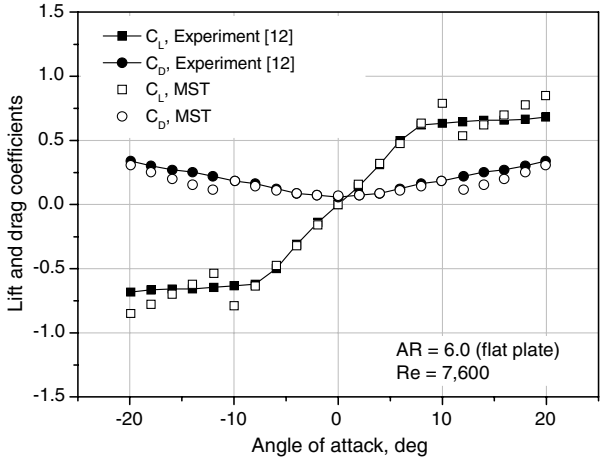

Fig. 3 Steady-state aerodynamic characteristics of the flat plate wing.

The aerodynamic forces applied on the strip should be expressed differently with respect to the flow conditions. Figure 2 shows the wing section aerodynamic forces as per the stall criteria. In the attached flow range (Fig. 2a) and the dynamic stall range (Fig. 2b), the modified aerodynamic forces are expressed by Eqs. (5–7). In the dynamic stall range, to take into account the unsteady aerodynamic characteristics of the leading-edge vortex [11], the direction of the leading-edge suction force is assumed to be perpendicular to the wing chord. The circulatory normal force is assumed to be applied at the $\frac{1}{3}$-chord location from the leading edge due to the movement of the aerodynamic center. In the poststall flow range (Fig. 2c), the aerodynamic forces are the same as those defined in MST. The whole wing's instantaneous lift, thrust, and moment can be obtained in the same manner as outlined in [6].

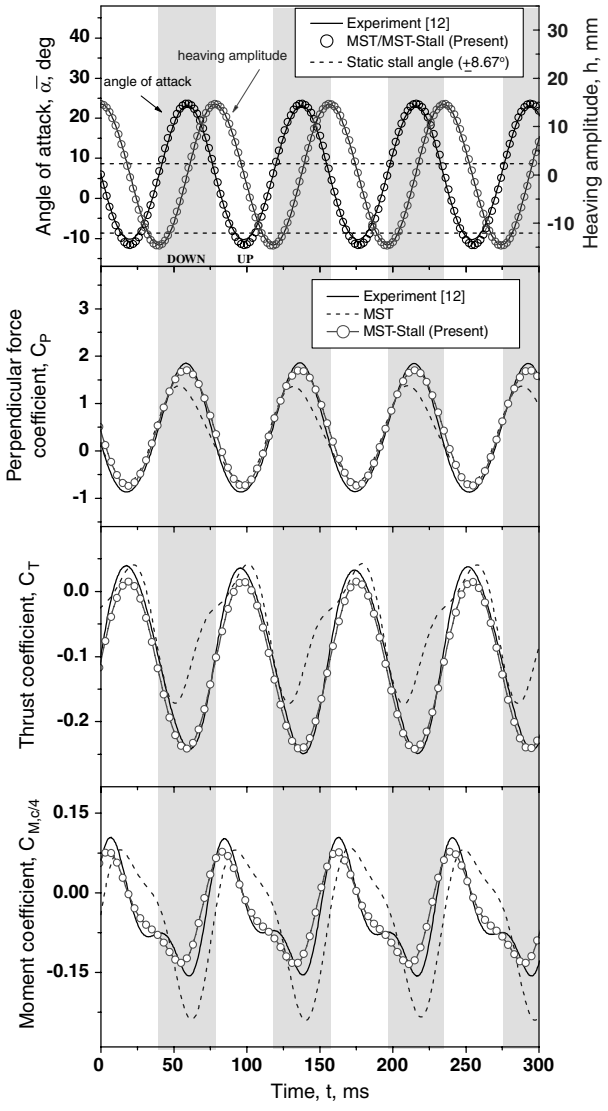

Fig. 4 Time histories of aerodynamic coefficients of the flat plate ($\theta = 6$ deg and $U = 3.7$ m/s).

III. Verification of Aerodynamic Model

A. Verification Model

To verify the aerodynamic model proposed in the present study, we compared the aerodynamic forces and moment calculated by using the improved aerodynamic model with the wind-tunnel test data obtained by Okamoto and Azuma for a finite rigid oscillating wing [12]. In the experiment, the wing was a flat plate with a wing aspect ratio of AR $= 6$, a wing chord of $c = 30$ mm, and a wing thickness of $t = 1.5$ mm, and the inflow speed was set to 3.7 m/s during the test.

B. Steady Aerodynamics

For the application of the aerodynamic models, the aerodynamic coefficients, η_s, $(C_d)_{\mathrm{cf}}$, and $(C_d)_f$, the zero-lift angle, and the maximum and minimum static stall angles should be defined before the unsteady aerodynamic analysis. These aerodynamic parameters can be determined by using the lift and drag coefficients measured in the steady aerodynamic test. In this study, we determined the aerodynamic parameters using the least-squares method to minimize the estimation errors, resulting in the following:

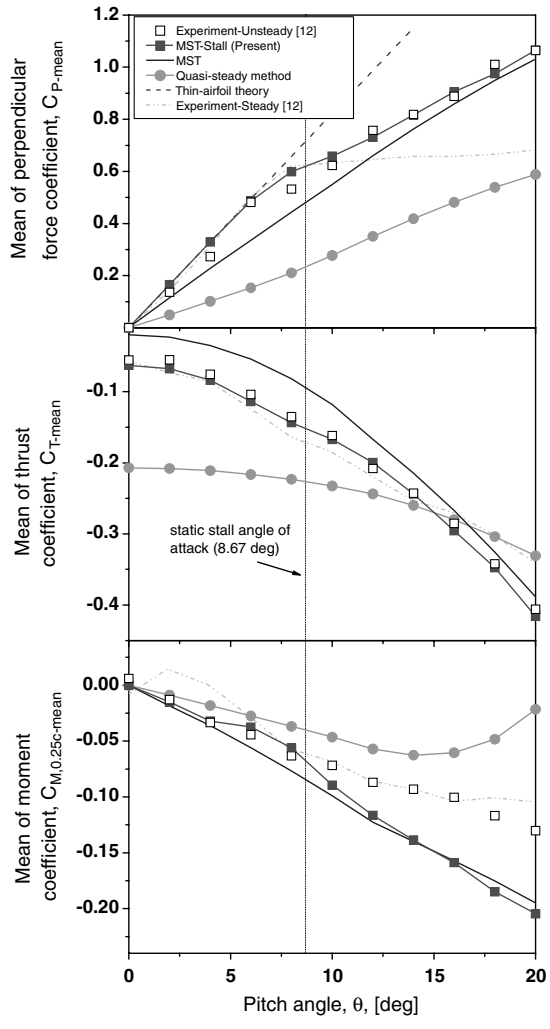

Fig. 5 Mean values of aerodynamic coefficients in unsteady state.

$$\eta_s = 0.18, \qquad (C_d)_{\text{cf}} = 2.65, \qquad (C_d)_f = 0.068$$
$$\alpha_0 = 0.0 \text{ deg}, \qquad (\alpha_{\text{stall}})_{\max} = 8.67 \text{ deg}$$
$$(\alpha_{\text{stall}})_{\min} = -8.67 \text{ deg} \tag{12}$$

Figure 3 shows the comparison between the MST and the experimental data. The results show good agreement in the lift and drag coefficients, especially within the fully attached flow range; however, in the region outside of the attached flow range, there are some discrepancies, which may be caused by the discontinuity characteristics of MST near the static stall angle.

C. Unsteady Aerodynamics

Using the determined aerodynamic parameters, we performed an unsteady aerodynamic analysis of the plate wing under the same test conditions: the heaving amplitude, $h_1 = 14.7$ mm, and the heaving motion frequency, $\omega = 80.16$ rad/s [12]. A low-pass filter with a cutoff frequency of 30 Hz was adopted in the data postprocessing, just as used in the experiment. To investigate the improvement of the aerodynamic model, we compared two kinds of aerodynamic models. The first model is the MST, which is the original MST, and the second one is MST-stall, which is proposed in this study.

Figure 4 shows the time histories of the resultant angle of attack $\bar{\alpha}$, the perpendicular force coefficient C_P, the thrust coefficient C_T, and the aerodynamic moment coefficient at the quarter-chord $C_{M,0.25c}$ when the pitch angle θ of the wing is fixed at 6° and the wing is oscillating in the vertical direction, resulting in a heaving motion. The resultant angle of attack $\bar{\alpha}$ can increase up to 23.2° in the middle of the downward stroke, and this angle of attack is almost three times higher than the static stall angle (8.67°); this high relative angle of attack causes the aerodynamic model (MST-stall) to overpass the dynamic stall range. During the upward stroke, the perpendicular force and thrust coefficients obtained by MST and MST-stall are in good agreement with the experimental data. During the downward stroke, however, there are significant discrepancies between the MST and the experimental data. In contrast with the MST results, the aerodynamic force and moment coefficients obtained from MST-stall show very good agreement with the experimental data during the entire stroke.

Figures 5 and 6 show more comparisons of MST and MST-stall models with the experimental data for various pitch angles from 0 to 20°, in terms of the mean and rms values. To specify the upper and lower boundaries of the unsteady aerodynamic coefficients, we also present the quasi-steady analysis results and the steady test data in the first plot of Fig. 5. For all the pitch angles, the mean values of C_P and C_T of MST-stall agree with the experimental data much better than those of MST and the quasi-steady method. The moment coefficient plot also shows that the MST-stall result is closer to the experimental data when the pitch angle is lower than the static stall angle. Figure 6 also shows that MST-stall presents more accurate RMS values of aerodynamic coefficients than other models.

The overall comparison results clearly confirm that the unsteady aerodynamic performance of a flapping wing can be more accurately predicted by MST-stall, especially when the pitch angle is less than the static stall angle. Because most biological and artificial flyers sustain the mean pitch angle less than the static stall angle during cruise flight, MST-stall is anticipated to be valuable for an efficient unsteady aerodynamic prediction of flapping flight.

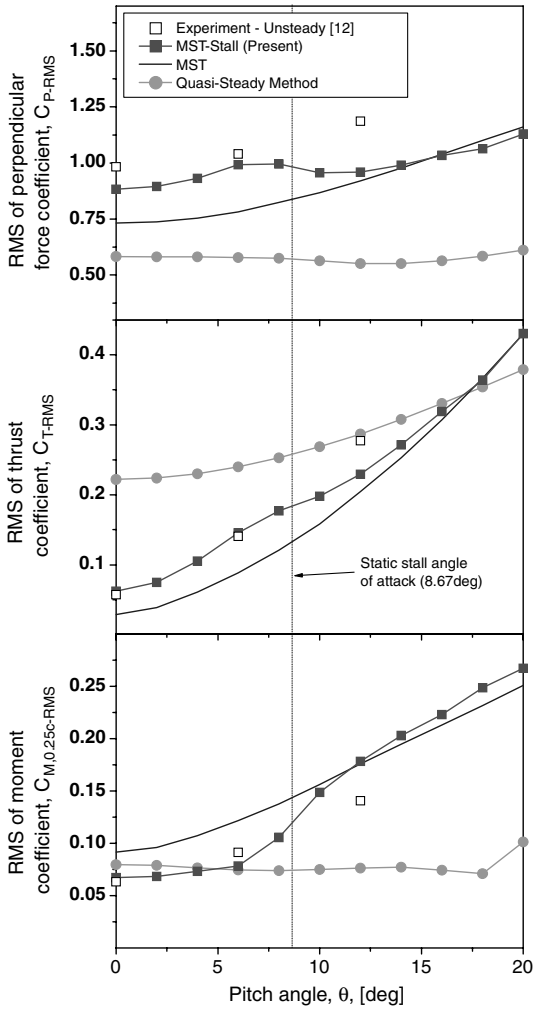

Fig. 6 RMS values of aerodynamic coefficients in unsteady state.

IV. Conclusions

In the present study, an unsteady aerodynamic model, MST-stall, was suggested for its efficient and practical application to the aerodynamic and aeroelastic analyses of flapping wings. The MST model was improved to consider dynamic stall for a high relative angle of attack. The dynamic stall model was proposed to consider the dynamic stall effects due to both the plunging and pitching motions, and the aerodynamic forces applied on the wing section were differently described according to the flow conditions. To investigate the accuracy and validity of MST-stall, the analysis results using MST and MST-stall were compared with the experimental data for an oscillating flat plate wing. The comparison results clearly showed that MST-stall can more accurately predict the unsteady aerodynamic loads of the oscillating finite wing. Because of the simplicity of the present model, MST-stall can be efficiently used in various time-consuming problems of flapping-wing flights, such as fluid–structure interaction, optimal flapping-wing design, and flapping-wing flight control.

Acknowledgments

This work was supported by a Korea Research Foundation Grant funded by the Korean Government (MOEHRD) (KRF-2007-313-D00122). The second author would like to thank the Brain Korea 21 Project in 2010. The authors would like to thank James D. DeLaurier of the University of Toronto and M. Okamoto of the Akita National College of Technology for their gracious support for this study. The authors also thank anonymous reviewers and the Editor for their valuable comments and suggestions.

References

[1] Deng, X., Schenato, L., Wu, W., and Sastry, S., "Flapping Flight for Biomimetic Robotic Insects: Part 1, System Modeling," *IEEE Transactions on Robotics and Automation*, Vol. 22, No. 4, 2006, pp. 776–788.
doi:10.1109/TRO.2006.875480

[2] Dickson, W. B., Straw, A. D., and Dickinson, M. H., "Integrative Model of *Drosophila* Flight," *AIAA Journal*, Vol. 46, No. 9, 2008, pp. 2150–2164.
doi:10.2514/1.29862

[3] Dietl, J. M., and Garcia, E., "Stability in Ornithopter Longitudinal

Flight Dynamics," *Journal of Guidance, Control, and Dynamics*, Vol. 31, No. 4, 2008, pp. 1157–1162.
doi:10.2514/1.33561

[4] Grauer, J. A., and Hubbard, J. E., "Multibody Model of An Ornithotper," *Journal of Guidance, Control, and Dynamics*, Vol. 32, No. 5, 2009, pp. 1675–1679.
doi:10.2514/1.43177

[5] Chung, S.-J., and Dorothy, M., "Neurobiologically Inspired Control of Engineered Flapping Flight," *Journal of Guidance, Control, and Dynamics*, Vol. 33, No. 2, 2010, pp. 440–453.
doi:10.2514/1.45311

[6] DeLaurier, J. D., "An Aerodynamic Model for Flapping-Wing Flight," *The Aeronautical Journal*, Vol. 97, No. 964, April 1993, pp. 125–130.

[7] Liu, H. T., "Unsteady Aerodynamics of a Wortmann Wing at Low Reynolds Numbers," *Journal of Aircraft*, Vol. 29, No. 4, 1992, pp. 532–539.
doi:10.2514/3.46198

[8] Prouty, R. W., *Helicopter Performance, Stability, and Control*, PWS Engineering, Boston, 1986, Chap. 6.

[9] Scherer, J. O., *Experimental and Theoretical Investigation of Large Amplitude Oscillating Foil Propulsion Systems*, Hydronautics, Laurel, MD, 1968, pp. 13–14.

[10] Larijani, R. F., and DeLaurier, J. D., "A Nonlinear Aeroelastic Model for the Study of Flapping Wing Flight," Progress in Astronautics and Aeronautics, Vol. 195, AIAA, Reston, VA, 2001, pp. 399–428.

[11] Kim, D.-K., Han, J.-H., and Kwon, K.-J., "Wind Tunnel Tests for a Flapping Wing Model with a Changeable Camber Using Macro-Fiber Composite Actuators," *Smart Materials and Structures*, Vol. 18, No. 2, 2009, Paper 024008.
doi:10.1088/0964-1726/18/2/024008

[12] Okamoto, M., and Azuma, A., "Experimental Study on Aerodynamic Characteristics of Unsteady Wings at Low Reynolds Number," *AIAA Journal*, Vol. 43, No. 12, 2005, pp. 2526–2536.
doi:10.2514/1.14813

P. Beran
Associate Editor